Available online at www.sciencedirect.com
SCIENCE DIRECT®
Electrochimica Acta 51 (2006) 1157–1164
ELECTROCHIMICA Acta
www.elsevier.com/locate/electacta

Anodically formed oxide films and oxygen reduction on electrodeposited ruthenium in acid solution

M. Metikoš-Huković [a,*,1], R. Babić [a], F. Jović [a], Z. Grubač [b]

[a] *Department of Electrochemistry, Faculty of Chemical Engineering and Technology, University of Zagreb, P.O. Box 177, 10000 Zagreb, Croatia*
[b] *Faculty of Chemical Technology, University of Split, N. Tesle 10 Split, Croatia*

Received 8 December 2004; received in revised form 4 February 2005; accepted 15 May 2005
Available online 1 July 2005

Abstract

The impedance of the anodically formed hydrous Ru oxide in the system Ru|oxide film|1 M $HClO_4$ solution has been studied in the range of potentials where the electrode process occurs by a double electron and proton exchange between the oxide film and the solution. The results allowed us to clearly distinguish between the surface process at higher frequency and the bulk process at lower frequency. The high-frequency charging is found to be coupled to Faradaic charging at the film/solution interface. Evaluation of the impedance data at lower frequency, using diffusion equations for the finite boundary conditions, yields an effective proton diffusion coefficient to be 10^{-10} to 10^{-11} $cm^2\,s^{-1}$.

Oxygen reduction on the spontaneously oxidized ruthenium electrode was discussed on the basis of a rotating ring-disk voltammetry.

Keywords: Ruthenium; Ruthenium oxides; Oxygen reduction; Rotating ring-disk electrode; Impedance spectroscopy; Cyclic voltammetry

1. Introduction

There has been a growing interest in the electrochemical properties of the ruthenium, especially due to the electrocatalytic properties of anodes based on Ru alloys with Pt or ruthenium oxides. RuO_2 films on Ti substrate, prepared by thermal decomposition of ruthenium salts, are known as dimensionally stable $RuO_2 \times TiO_2$ anodes of excellent stability and low overvoltage for the evolution of chlorine [1]. Ruthenium hydrous oxides, especially those formed by the sol–gel or the electrochemical processes, distinguish themselves from other transition metal oxides by their exceptionally high-charge storage capacity [2–5], due to the high electron and proton conductivity, together with a high degree of reversibility of the redox processes which take place over a large range of potentials. Several studies of oxygen reduction on a ruthenium electrode have shown its considerable affinity for the oxygen reduction in both acid [6–8] and alkaline electrolytes [9–11]. The electrocatalytic reduction of oxygen plays a major role in several industrial processes and in corrosion and corrosion protection [1,12]. Pt–Ru alloy is preferred over platinum as a better promoter of the oxidation of small organic molecules [13]. For many of the above applications, the ruthenium or ruthenium oxide coatings appear to be more desirable and suitable [2] than the bulk metal. Electrochemical deposition of ruthenium on various substrates and anodic oxidation of deposited ruthenium is a well-known method for the preparation of ruthenium oxide coating [4,5,14–25]. Conway et al. [14–16], Burke and co-workers [17,18,25] and Michell et al. [19] frequently used cyclic voltammetry (CV) and other polarization techniques to investigate the surface properties of electrodeposited ruthenium. They showed that the continuous potential cycling into the oxide region up to 1.4 V led to a modification of the oxide film accompanied by the enhanced electrocatalytic efficiency in the evolution of chlorine and oxygen. Vuković et al. [20–22] have shown that the electrodeposited ruthenium layer contains a significant amount of physically adsorbed and chemisorbed water, and that the modification of the oxide film caused by the continuous cycling of the potential is due to an increase in the

* Corresponding author. Tel.: +385 1 4597140; fax: +385 1 4597139.
E-mail address: mmetik@marie.fkit.hr (M. Metikoš-Huković).
[1] ISE member.

0013-4686/$ – see front matter © 2005 Elsevier Ltd. All rights reserved.
doi:10.1016/j.electacta.2005.05.029

number of hydroxyl groups in the film. The electrochemical impedance spectroscopy (EIS), which has been considered a powerful in situ diagnostic technique in separating different rate processes in the frequency domain, has been used in studying the electrochemical properties of the hydrous ruthenium oxide film [23,24].

The electrochemical behavior of the electrodeposited Ru/$HClO_4$ solution (1 mol dm^{-3}), in the range of potentials between hydrogen and oxygen evolution, was studied under potentiodynamic and potentiostatic experimental conditions using CV and EIS. In this work, we aimed at studying the interfacial and bulk solid-state redox charging processes in the investigated system using EIS. Potentiostatic experiments conducted in the frequency domain of 6 decades enable us to clearly distinguish the slower potential-dependent charging processes, i.e. the variations of the proton transport rate with applied potential in Ru oxide films from the faster processes related to the charging at the film/solution interface.

The electrocatalytic affinity of the electrodeposited Ru films towards the oxygen reduction reaction (ORR) was investigated using the ring-disk electrode. The study was a part of our broader investigation of the ORR on Pt, Pt–Ru electrodes as well as on Pt–Ru/Vulcan fuel cell catalysts.

2. Experimental

2.1. Cyclic voltammetry and EIS measurements

A disk-shaped electrode, made from spectrographically pure gold (Johnson & Matthey) with a geometrical surface of 0.071 cm^2, served as the support for deposition of ruthenium films. Before electrodeposition, the gold electrode was mechanically and electrochemically treated. Mechanical treatment consisted of polishing using Al_2O_3 granules of fine sizes (1, 0.3 and 0.05 μm) up to a mirror finish. The electrode was degreased with ethanol and rinsed with deionized water in an ultrasound bath. The electrochemical treatment consisted of potential cycling, within the potential range from 0 to 1.8 V versus SHE, with a scan rate of 100 mV s^{-1}, until a reproducible potentiodynamic profile was reached for the Au electrode.

Ruthenium deposition was performed from 2×10^{-3} mol dm^{-3} $RuCl_3$ in 1 mol dm^{-3} $HClO_4$ at a constant potential of 0.05 V versus SHE for a period of 1500 s. The reference electrode during deposition was Ag/AgCl electrode immersed in 3 mol dm^{-3} KNO_3 solution (Radiometer analytical), while the platinum foil served as the counter electrode. Freshly deposited electrodes were rinsed in order to remove the rest of the deposition solution and transferred to an electrochemical cell containing 1 mol dm^{-3} $HClO_4$ (pH 0) deaerated by continual flow of N_2 (99.99%). The electrodes were treated by repetitive cycling (50 cycles) over the potential range 0.05–0.85 V versus SHE with a scan rate of 100 mV s^{-1} with the objective of cleaning the surface and reaching stationary conditions. Then, the electrode was held at −0.13 V for 60 s in order to remove completely the possible surface oxides. Finally, the samples were potentiodynamically polarized (10 mV s^{-1}) to the potential of 0.05 V, which was the initial potential for CV measurements. For impedance measurements, the samples were potentiodynamically polarized (10 mV s^{-1}) to the desired potential and after a 60 s wait period, impedance data were collected. Measurements were performed with the ac voltage amplitude ±5 mV in the frequency range from 40 mHz to 50 kHz. Both CV and EIS measurements were performed in a standard three-electrode electrochemical cell. A thin platinum electrode was used as the counter electrode and a saturated Hg/$HgSO_4$ electrode, whose potential was 0.658 V versus SHE, as the standard electrode. A PAR EG&G potentiostat (model 273) and a PAR EG&G lock-in amplifier (model 5301A) controlled by a PC were used.

2.2. RRDE measurements

RRDE measurements were carried out using the ring-disk electrode assembly, Model EAD 10000. Both the disk and ring were made of platinum. The disk surface area was 0.1257 cm^2. Ruthenium deposition on the disk was performed under the same condition as on the gold electrode. During ruthenium deposition on the disk electrode, the ring electrode was held at 0.84 V versus SHE in order to prevent ruthenium underpotential deposition on it. The RRDE collection efficiency, N, was determined to be 0.24 from the slope of the disk currents, j_D, against ring currents, j_R, at different rotation rates using 10^{-3} mol dm^{-3} $K_3Fe(CN)_6$ in 0.5 mol dm^{-3} K_2SO_4. The potentiostat used for the ring-disk measurements was a Electrolab BPG-200 bipotentiostat with a built-in sweep generator. A platinum foil was used as a counter electrode and the saturated calomel electrode as the reference electrode. The disk was polarized over the potential range 0.80–0.10 V with a scan rate 5 mV s^{-1} and a rotation rate from 1000 to 6000 rpm. The ring potential was kept at 1.2 V versus SHE to oxidize peroxide at the mass transport limiting rate.

All measurements were performed at room temperature (21 ± 2 °C) and potential values in the paper refer to the SHE.

3. Results and discussion

3.1. Cyclic voltammetry

A family of the cyclic voltammograms of the deposited ruthenium electrode taken at a sweep rate of 10 mV s^{-1} in 1 mol dm^3 $HClO_4$ is shown in Fig. 1a and b. The anodic limit was increased progressively with each sweep from 0.80 to 1.30 V and the electrode was held at the cathodic limit (E = −0.13 V) to allow the complete reduction between each sweep. The CV features in figures are in agreement with literature data [14–19,25], which indicate that the overall electro-oxidation/electro-reduction can be split into a number

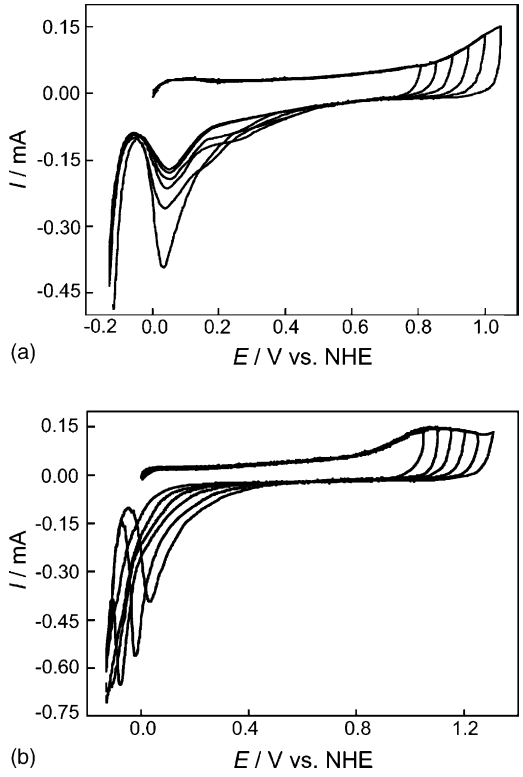

Fig. 1. CVs for a plated Ru deposit measured in 1 M $HClO_4$ at various sweep reversals: (a) from 0.8 to 1.05 V and (b) from 1.05 to 1.3 V; $\nu = 10\,mV\,s^{-1}$.

of reactions. They will be presented in short. On the positive going potential sweep, there is the hydrogen region which overlaps with ruthenium oxidation [14,15,18,19,26]. The slightly pronounced current plateau between ca. 0.2 and 0.7 V formed during the electrode linear polarization is due to the formation of a surface oxide film [14–19,25,27]. Since the corresponding cathodic branch of the CV shows two current maxima, it seems that the anodic plateau was formed by overlapping two stages of the surface oxidation (Ru(I) and Ru(II)) as was suggested by Conway and co-workers [14,15]. The oxidation state of ruthenium in the oxide is two at the end of this potential region, i.e. ruthenium oxide exists as hydrated RuO [19], $Ru(OH)_2$ or $RuO \times H_2O$ [28]. Further increase in current, which occurs by increasing anodic-potential limit, corresponds to the formation of ruthenium oxides where ruthenium is of higher oxidation states. Burke and co-workers [17,18] proposed that the slight increase in oxidation current from 0.7 to ca. 1.0 V is possible due to the formation of RuOOH (Ru_2O_3). The standard electrode potential of Ru/Ru_2O_3 couple equals to 0.738 V [29]. Its formation in that potential range on the deposited ruthenium electrode was proposed also by other authors [20,22,28,30]. Fig. 1a shows that the oxide layers formed on the ruthenium-deposited electrode in the potential range 0.8–1.0 V give cathodic sweeps with two current maxima. The first, slightly pronounced current peak shifts to more cathodic values with increasing anodic-potential limit, while the second and more pronounced current peak remains at the same potential (ca. 0.05 V). When anodic limit potential equals 1.05 V, merging of both cathodic current maxima into one maximum is observed in the cathodic cycle.

Fig. 1b shows that the anodic current decreases beyond 1.05 V due to the electrode passivation and formation of hydrous RuO_2. After oxidation of the deposited ruthenium from 1.05 to 1.15 V, the cathodic sweep shows a well pronounced current peak corresponding to the oxide film reduction, which shifts towards cathodic potential values with the shift of the anodic limit to more positive potentials. Beyond 1.2 V, the anodic current starts to increase due to both oxygen evolution and ruthenium dissolution, where ruthenium species bearing Ru oxidation states up to +8 (RuO_4) are involved [27,28]. When the electrode has been oxidized to $\geq$1.35 V, there is almost no oxide film reduction peak on the cathodic sweep; the oxide film reduction is only completed in the hydrogen region. Since the current, during the forward and reversal potential scan, is not influenced by the electrode rotation, it is proposed that the hydrogen and oxygen species diffuse into and out of the oxide layer. Details to this point will be discussed along with the results of the EIS experiments.

The irreversibility in the formation and reduction of the ruthenium oxide films, which increases with increasing anodic potential, is linked to their intrinsic structures. XPS results obtained by Hu et al. [5] showed that the irreducible oxide was composed of an aggregate consisting of Ru in various oxidation states, bridged oxygen, OH and water in a 3D-like structure which is relatively ordered and compact.

3.2. Electrochemical impedance spectroscopy

A typical set of impedance spectra recorded on the deposited ruthenium electrode potentiostatically oxidized at potentials between 0.3 and 1.1 V, presented as Bode plots, is shown in Fig. 2. The modeling procedure for the impedance frequency responses is given in the appropriate description of relevant surface and bulk redox processes involved in the system investigated. The Faradaic process

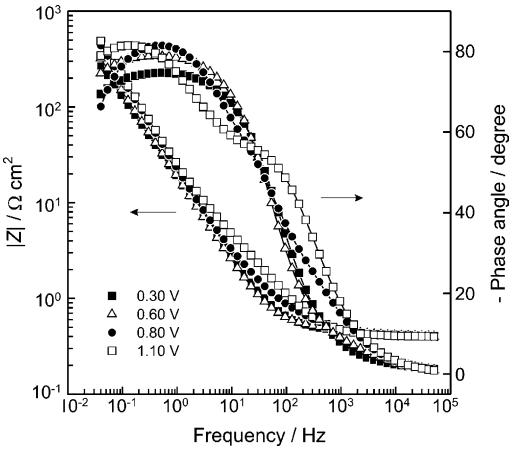

Fig. 2. Bode plots for a plated Ru deposit in 1 M $HClO_4$ at specified potentials.

of the electrochemical reactivity of hydrous oxides in the investigated potential range varies strongly, depending on the extent of coupling between the internal redox system of the oxide and the redox system at the oxide/solution interface. The activity of this redox system depends, in turn, on the rate of double electron–proton injection process into a hydrous Ru oxide according to Eq. (1):

$$RuO_{(x+\delta)}(H_2O)_{(y-\delta)} + 2\delta H^+ + 2\delta e^- \Leftrightarrow RuO_x(H_2O)_y, \quad (1)$$

i.e. a hydrogen atom is incorporated into a hydrous oxide by injection of an electron from the ohmic contact and a proton from solution, thus lowering the formal oxidation state of Ru by one unit. The reverse electro-oxidative process involves the double ejection of an electron and a proton from a hydrous oxide. While this process is very fast for surface sites located in easily accessible regions, the proton incorporation in regions with difficult access creates a slow diffusion-controlled process. Slow diffusion-controlled proton penetration has been shown to occur using diverse techniques such as potential pulse [31,32], current pulse [33] spectroelectrochemistry [34] and impedance analysis [23,24].

In order to model the impedance data for the above process (Fig. 2), the following important aspects of the potential dependence of the Ru oxide film must be considered: (i) the pseudocapacitive nature of the electrode process occurring at the surface of Ru oxide under the conditions of our experiments according to the relation (1); (ii) the interfacial transfer processes, one is an electron transfer at the electrode/film (M/F) and the other is an ion transfer at the solution/film interface (F/S); (iii) the charge transport within the film. As resistance does not appear to depend on the oxide film properties, the impact of the R_F on the observations is ignored in the present discussion.

Two approaches were taken in this work to understand and interpret the impedance data given in Fig. 2. The first one involved identifying the best-fit electric equivalent circuit (EEC), based on Boucamp's software [35], in order to establish the values of circuit elements. The intention of this work was then to correlate their values with cyclic voltammetry data as a function of the applied potential. The usual guidelines for the selection of the best-fit EEC were followed: (i) a minimum number of circuit elements are to be employed;

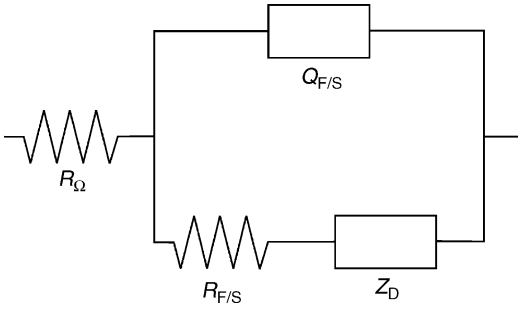

Fig. 3. The electrical equivalent circuit used to fit the impedance spectra.

(ii) the χ^2 error is suitably low ($\chi^2 \leq 10^{-4}$) and the errors associated with each element are up to 5%. Many EEC were examined, but only the one shown in Fig. 3 obeyed these criteria. Also, this EEC fits well to the impedance data obtained at various potentials in 1 mol dm^{-3} $HClO_4$ solution. Fig. 2 depicts the overlay of the experimental (at the selected potentials) and the calculated Bode data shown in Table 1, using the EEC in Fig. 3. The EEC in Fig. 3 is also applicable to the thin film-modified electrodes (oxides and conducting polymers) if the conventional semi-infinite Warburg impedance is replaced with a finite Warburg term [36] or a finite length transmission line [23,37–40]. The meaning of the parameters in the EEC is as follows:

- R_Ω represents the serial sum of all resistance at the F/S interface, i.e. the charge transfer resistance (R_{ct}), the oxide film resistance (R_F), the proton transfer resistance (R_{pt}) and the electrolyte resistance (R_{el}), in which the R_{el} dominates the serial sum.
- $C_{F/S}$ is the total film/solution interfacial capacitance ($C_{F/S}$). It represents the parallel sum of the pseudocapacitance (C_ϕ) and the double layer capacitance (C_{dl}).
- Serial combination of the surface resistance R_ϕ corresponding to the surface redox process and the transmission line-like impedance (Z_D) represents the impedance due to a slow charging/discharging process in the bulk of the oxide film, occurring through the Faradaic charge transfer and restricted diffusion of protons within the bulk of the film.

Table 1
Impedance parameter values of the deposited ruthenium electrode at different potentials in 1 mol dm^{-3} $HClO_4$

E (V)	$10^3 \times Q_{F/S}$ (Ω^{-1} cm^2 s^n)	n	$10^2 \times R_\phi$ (Ω cm^2)	R_D (Ω cm^2)	$10^2 \times \tau_D$ (s)	$10^3 \times C_T$ (F cm^{-2})
0.30	10.4	0.80	4.8	1.30	0.19	11.9
0.40	10.6	0.81	9.3	0.98	0.11	11.7
0.50	10.1	0.82	12.4	0.69	0.11	11.7
0.60	7.5	0.82	12.1	0.74	0.23	10.6
0.70	5.9	0.82	7.0	3.11	1.05	9.3
0.80	5.1	0.82	6.0	5.08	1.59	8.2
0.90	4.0	0.84	18.0	8.73	3.19	7.7
1.00	4.2	0.83	50.0	27.49	8.82	7.4
1.08	4.8	0.83	368.0	67.01	12.04	6.6

$R_\Omega = 0.41\ \Omega\ cm^2$.

The overall impedance of the equivalent circuit as a function of frequency was calculated according to Eq. (2):

$$Z(\omega) = \frac{R_\Omega + (R_\phi + Z_D)}{[1 + (R_\phi + Z_D) j\omega C_{dl}]} \quad (2)$$

where ω is the angular velocity and j is $(-1)^{1/2}$. It should be noted that EIS was unable to distinguish between the double layer capacitance (C_{dl}) and the pseudocapacitance (C_ϕ) charging modes of the Ru oxide films. Thus, in Eq. (2), instead of C_{dl}, the value of $C_{F/S}$ is introduced.

The high-frequency impedance (Z_{HF}) is given by Eq. (3):

$$Z_{HF}(\omega) = \frac{R_\Omega + 1}{(j\omega)^n Q_{F/S}} \quad (3)$$

where the frequency-independent impedance parameters $Q_{F/S}$ and n, describing the impedance of a constant phase element, are introduced instead of the film/solution interfacial capacitance ($C_{F/S}$) due to the non-ideality of the solid electrode surface response [41].

The frequency dependence of the so-called transmission line-like impedance elements is given by Eq. (4):

$$Z_D(\omega) = R_D(j\omega\tau_D)^{-1/2} ctnh\ (j\omega\tau_D)^{1/2} \quad (4)$$

where τ_D represents the diffusion time constant related to the diffusion resistance, R_D, and the internal capacitance, C_D, $\tau_D = R_D C_D$.

According to Eqs. (2)–(4), the overall electrode impedance is described by six frequency-independent parameters, three of which (R_Ω, $Q_{F/S}$ and n) describe the fast electrode process dominating at higher frequencies, while the other three (R_ϕ, R_D and τ_D) describe the slow electrode process that dominates at low frequencies. Their values, as a function of film formation potential (E_f), are given in Table 1. The high-frequency resistance R_Ω, that is equal to $0.41\,\Omega\,cm^2$, does not depend on the electrode potential and presents the electrolyte resistance. The high-frequency capacitance is presented by a constant phase element (CPE) which generates an impedance $Z_{CPE} = [Q_{F/S}(j\omega)^n]^{-1}$. The CPE has no physical meaning, but allows an evaluation that indicates the degree of system complexity. Hence, the CPE represents the deviations observed from the ideal capacitor, such as slope in plot log $|Z|$ versus log f smaller than -1 and a phase angle in plot θ versus log f smaller than -90°, respectively. The value of n associated with CPE, greater than 0.80, indicates that CPE behaves as a capacitor, hence it can be assumed that $Q_{F/S} \cong C_{F/S}$. Data in Table 1 show that $C_{F/S}$ values are rather high (4–11 mF cm^{-2}) and decrease with increasing anodic potential. Since $C_{F/S}$ values are much higher than ordinary C_{dl} values for plane, compact oxide electrodes [42], it may be assumed that $C_{F/S} \cong C_\phi$. The decrease of C_ϕ values with increasing E_f points to a certain extent of surface area reduction due to the formation of less hydrous and more compact oxide films.

The values of R_ϕ, τ_D and R_D depend on the thickness and the structure of the oxide film. The most important structural parameters are the concentration of the protons as diffusing species and their diffusion coefficient. The oxide films with higher thickness, lower concentration of protons and lower diffusion coefficient will have higher values of these parameters. An increase of these parameters generally denotes an increase in the inhibition of the film equilibration, once the electrode has been polarized. Table 1 shows that these values, particularly those of R_D and τ_D increase (except from 0.3 to 0.4 V) with increasing E_f. Oxide films grown on Ru by constant potential anodization reach a thickness of up to 30 nm [23]. Taking into account this thickness and applying the relation $\tau_D = L^2/D$, where L is the thickness of the oxide layer, the diffusion coefficient of protons (D) can be estimated. The values obtained are between 10^{-10} and 10^{-11} cm^2 s^{-1} depending on E_f. With increasing E_f, the proton diffusion coefficient decreases due to the change in film structure that becomes less amorphous and more compact at higher anodic potentials. The other factor that influences the change in D values is the change in a film thickness with increasing E_f. Optical measurements [23] as well as potentiodynamic [17] measurements indicate that the film thickness increases with increasing E_f. For the oxide film on ruthenized gold, Rishpon and Gottesfeld [23] calculated an effective diffusion coefficient of protons to be between 10^{-11} and 10^{-12} cm^2 s^{-1}. For thermally prepared RuO_2 films, the experimentally determined values for diffusion coefficient of protons differ significantly, depending upon the layer preparation. Using ac impedance studies Raistrick and Sherman [43] and Tsai and Rajeshwar [44] estimated a diffusion coefficient of protons to be 10^{-10} cm^2 s^{-1}. Conway et al., investigating a self-discharge of a thermally prepared electrode, estimated the proton diffusion coefficient to be around 10^{-12} cm^2 s^{-1}, while Weston and Steele [32], using current transient measurements, obtained the values between 10^{-14} and 10^{-15} cm^2 s^{-1}. Generally, the charging of the grain surface, which requires only the transport of protons along aqueous pores, may be associated with a much higher proton diffusion coefficient than the charging of the bulk of oxide grains. The proton diffusion coefficient estimated in this work correlates well with values given in literature. Our results suggest that the main reason for the observed increase of R_D and τ_D is a change in the oxide structure and a decreasing concentration of the protons inside the oxide layer due to the lower content of the proton-donating species such as H_2O and OH. The values of R_D and τ_D can be grouped into three regions: the first one with very low values of R_D and τ_D in the potential range from 0.3 to 0.6 V, where the oxide layer exists as hydrated RuO. An increase in R_D and τ_D is observed in the potential region from 0.7 to 0.9 V, where hydrated RuO undergoes further oxidation to RuOOH (Ru_2O_3). Finally, oxidation of Ru(III) oxide layer to RuO_2 is accompanied with a significant increase in all three impedance parameters, R_S, R_D and τ_D.

An insight into the content of proton-donating species could also be obtained from the values of total capacitance, C_T, equal to: $C_T = C_\phi + C_D$. The C_T values were calculated

under the assumption that $Q_{F/S} \approx C_\phi$ because $Q_{F/S} \gg C_{dl}$, while C_D values were calculated from the τ_D and R_D values. The value of C_T is also presented in Table 1 as a function of E_f. The C_T decreases with increasing E_f suggesting a loss of reaction sites caused by the formation of the oxide films in which the oxidation state of Ru increases. Our results also show that the Faradaic pseudocapacitance (C_ϕ) dominates the total film capacitance of oxide layers prepared at lower potential values; when increasing the film formation potential, its fraction in the total capacitance decreases. All impedance results indicate that anodic oxidation at lower potential values produces more porous and more open oxide films, i.e. the films that are more hydrous or amorphous, at least in their surface region. Oxide films formed at higher anodic potentials are characterized by a reduced surface area, they are less hydrous and/or their structure is more crystalline.

3.3. Oxygen reduction

Rotating ring-disk experiments were performed to measure the amount of H_2O_2 species formed as an intermediate or to confirm that O_2 is directly reduced to water in a four-electron process. Fig. 4 shows a typical result obtained on a rotating ruthenium-deposited electrode as a function of the potential and rotation rate. A platinum ring, potentiostated at $E = 1.2$ V, was used to monitor the formation of the hydrogen peroxide. The S-shaped disk current, j_D, and its dependence upon the rotation rate indicates that the reaction is under mixed activation–diffusion control at all rotation rates examined. The ring current, j_R, which corresponds to the diffusion-controlled oxidation of peroxide is very small indicating that the O_2 reduction on the disk proceeds as a four-electron process. The amount of hydrogen peroxide can be calculated using the detected ring currents and disk currents normalized for the collection efficiency, N:

$$\%H_2O_2 = \frac{100\, j_R}{j_R + N j_D} \tag{5}$$

The calculation shows that the amount of H_2O_2 decreases with increasing cathodic potential: at ~0.6 V, it approaches 6% and drops to ~2% at 0.1 V. Thus, the main reaction at the disk electrode involves the four-electron overall reduction. For a rotating disk electrode experiment involving an electrode process, which is first order in reactant, the observed current is given by Koutecky–Levich Eq. (6) [45]:

$$\frac{1}{j} = \frac{1}{j_k} + \frac{1}{j_L} \tag{6}$$

where j_k is the kinetic current and j_L is the corresponding diffusion limiting current equal to $B\omega^{1/2}$, where B is the constant. The plots of $1/j$ versus $\omega^{1/2}$, assuming a uniform current distribution, should yield parallel straight lines with the intercepts corresponding to j_k and the slope yielding the value of B.

The parameter B can be calculated from Eq. (7) [45]:

$$B = 0.62 n F D^{2/3} \nu^{-1/6} c(O_2) \tag{7}$$

where F is the Faraday constant (96,490 C mol^{-1}), D the molecular diffusion coefficient of oxygen in 1 mol dm^{-3} perchloric acid (1.1×10^{-5} cm^2 s^{-1}), ν the kinematic viscosity (0.01 cm^2 s^{-1}) and $c(O_2)$ is the bulk concentration of dissolved oxygen (1.6×10^{-6} mol cm^{-3}) [46]. When $n = 4$, $B = 0.132$ mA cm^{-2} (rpm)$^{-1/2}$.

The linearity and parallelism of the plots obtained when data from Fig. 4 were plotted as $1/j$ versus $\omega^{-1/2}$ confirm that the kinetics are first order with respect to oxygen and that Eq. (6) is applicable. The average experimental value of B obtained from these plots is 0.13 mA cm^{-2} (rpm)$^{-1/2}$, which is in good agreement with the calculated value. This indicates that the oxygen reduction proceeds by an overall four-electron transfer process, i.e. $O_2 + 4H^+ + 4e^- \rightarrow 2H_2O$.

The Tafel slope could be obtained from the mass transfer-corrected plot E versus log $[jj_L/(j_L - j)]$ [47]. The value for Tafel slope that equals −124 mV dec^{-1} is obtained from this plot in the potential range from 0.77 to 0.64 V. The obtained value is not far from −118 mV dec^{-1} ($-2.3 \times 2RT/F$), which corresponds to the mechanism that involves one-electron discharge-determining step. Such data allow us to conclude that the product of the rate-determining step in the ORR is the electro-reduced adsorbed $(O_2^-)_{ads}$ species, i.e. $(O_2)_{ads} + e^- \rightarrow (O_2^-)_{ads}$. Between 0.6 and 0.4 V, the slope is −190 mV dec^{-1} and below 0.4 V, the current approaches limiting values. The obtained values are close to those found on platinum in acid media [46]. However, Tafel slopes higher

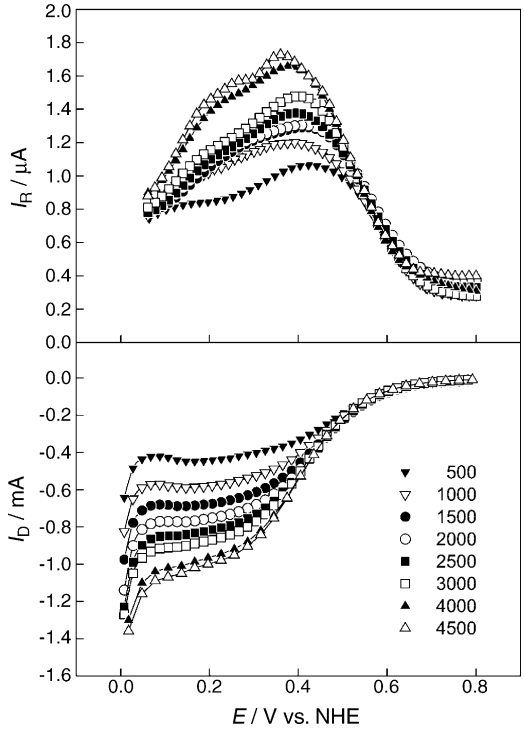

Fig. 4. Rotating disk-ring currents during the ORR on a plated Ru deposit at specified rotation rates (rpm) in 1 M $HClO_4$; $\nu = 5$ mV s^{-1}. Ring potential, $E = 1.2$ V vs. SHE.

than $-120\,\mathrm{V\,dec^{-1}}$ are often observed in reactions through some adsorbed layers at the surface. It is quite clear that a thin layer of ruthenium oxide, which exists in the mentioned potential range, could cause an increase in the Tafel slope.

To gain more insight into the kinetics of oxygen reduction on ruthenium-deposited electrode, the RRDE measurements were analyzed on the basis of the simple model proposed by Damjanovic et al. [48].

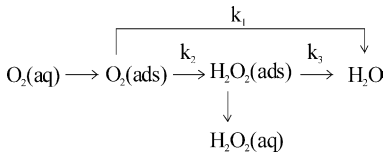

The model assumes: (i) no catalytic decomposition of hydrogen peroxide; (ii) adsorption/desorption of hydrogen peroxide is fast and in equilibrium; (iii) the rate constant for the hydrogen peroxide oxidation is negligible. The disk-ring data analysis reported by Hsueh et al. [47] could be used to derive a mathematical expression which would permit the calculation of the rate constants for the intermediate steps for the ORR. The main feature of the analysis is plotting $j_{DL}/(j_{DL}-j_D)$ versus $\omega^{-1/2}$ at a constant potential, where j_{DL} is the limiting current at the disk electrode. This plot is linear and adopts the same form, independently of the reaction scheme, provided that no catalytic decomposition of hydrogen peroxide occurs at the electrode surface. Fig. 5 shows that there is a linear dependence of the plot $j_{DL}/(j_{DL}-j_D)$ versus $\omega^{-1/2}$ upon the electrode potentials. Such dependence suggests that the ORR proceeds without catalytic decomposition of the hydrogen peroxide and that the model proposed by Damjanovic et al. [48] could be applied. The rate constants according to Hsueh et al. [46] are given by Eqs. (9)–(11):

$$k_1 = \frac{m_2 Z_1 (I_1 N - 1)}{(I_1 N + 1)} \tag{9}$$

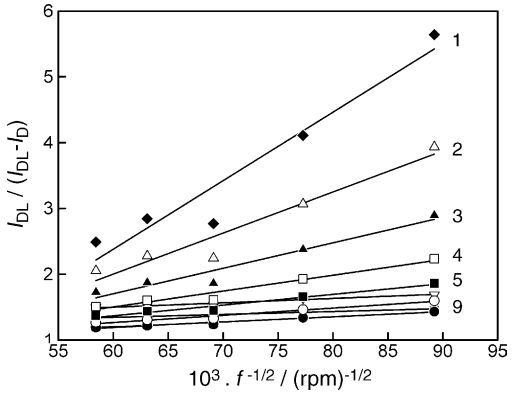

Fig. 5. The $j_{DL}/(j_{DL}-j_D)$ as a function of rotation rate at different potentials: (1) 0.400 V, (2) 0.425 V, (3) 0.450 V, (4) 0.475 V, (5) 0.500 V, (6) 0.525 V, (7) 0.550 V, (8) 0.575 V, (9) 0.600 V.

$$k_2 = \frac{2 Z_1 m_2}{(I_1 N + 1)} \tag{10}$$

$$k_3 = \frac{Z_2 N m_1}{(I_1 N + 1)} \tag{11}$$

where $Z_1 = 0.62\,D^{2/3}(O_2)\,\nu^{-1/6}$; $Z_2 = 0.62\,D^{2/3}(H_2O_2)\,\nu^{-1/6}$, $D(H_2O_2) = 6.8\times10^{-6}\,\mathrm{cm^2\,s^{-1}}$; I_1 and m_1 are the intercepts and slope of the plot of j_D/j_R versus $\omega^{-1/2}$, respectively; m_2 is the slope of the plot $j_{DL}/(j_{DL}-j_D)$ versus $\omega^{-1/2}$ and N is the electrode collection factor. The results showed that when j_D/j_R versus $\omega^{-1/2}$ is plotted at different electrode potentials (in the range from 0.4 to 0.6 V), a linear behavior is obtained with both the intercept and slope being dependent upon the electrode potential. At potentials below 0.4 V, the reproducibility of the experiments was relatively poor, which prevented us from analyzing such data. According to Damjanovic et al. [48], the type of j_D/j_R versus $\omega^{-1/2}$ dependence obtained suggests that all three reactions occur in the model. Within the above mentioned potential range, k_1 exponentially decreases from 2.5×10^{-2} to $4\times10^{-3}\,\mathrm{cm\,s^{-1}}$, while k_2 does not depend upon the potential and is equal to $5\times10^{-4}\,\mathrm{cm\,s^{-1}}$. Since the k_1 is much larger than k_2 over the potential range explored, oxygen is mainly reduced to water through the four-electron transfer reaction. The value of k_3 is of the order of $10^{-3}\,\mathrm{cm\,s^{-1}}$ and slightly increases with the potential. It is larger than k_2, indicating that the formation of hydrogen peroxide is a slow process in the series of the ORR steps.

4. Conclusions

Oxide films anodically formed on electrodeposited ruthenium are investigated by impedance spectroscopy. The results are discussed in terms of the formation and reduction of the phase oxides in the anodic film by mechanism involving the double ejection and injection of electrons and protons, with corresponding changes in the valence state of the ruthenium atom. The time-dependent information obtained from in situ EIS measurements showed that the processes in the system Ru/oxide film/solution are kinetically limited by diffusion of protons within the hydrous oxide film. Using equations for the finite boundary conditions, which is equivalent from an electrical point of view to the impedance of a finite transmission line, an effective diffusion coefficient of 10^{-10} to $10^{-11}\,\mathrm{cm^2\,s^{-1}}$ is obtained. The high-frequency charging is found to be coupled to Faradaic charging at the film/solution interface.

The ORR was investigated on sponataneosly oxidized electrodeposited ruthenium using ring-disk technique. The ORR proceeds mostly via four-electron transfer reaction to water with the formation of a small percentage of hydrogen peroxide. The rate constants for the oxygen reduction according to the Damjanovic reaction scheme were evaluated.

References

[1] K. Kinoshita, Electrochemical Oxygen Technology, Wiley, NY, 1992.
[2] S. Trasatti, Electrochim. Acta 36 (1991) 225.
[3] B.E. Conway, J. Electrochem. Soc. 138 (1991) 1539.
[4] T. Liu, W.G. Pell, B.E. Conway, Electrochim. Acta 42 (1997) 3541.
[5] C.-C. Hu, H.-R. Chiang, C.-C. Wang, J. Solid State Electrochem. 7 (2003) 477.
[6] S. Duron, R. Rivera-Noriega, P. Nkeng, G. Poillerat, O. Solorza-Feria, J. Electroanal. Chem. 566 (2004) 281.
[7] H. Inoue, S.R. Branković, J.X. Wang, R.R. Adžić, Electrochim. Acta 47 (2002) 3777.
[8] N.A. Anastasijević, Z.M. Dimitrijević, R.R. Adžić, Electrochim. Acta 31 (1986) 1125.
[9] J. Prakash, H. Joachin, Electrochim. Acta 45 (2000) 2289.
[10] N.A. Anastasijević, Z.M. Dimitrijević, R.R. Adžić, Electrochim. Acta 37 (1992) 457.
[11] N.A. Anastasijević, Z.M. Dimitrijević, R.R. Adžić, J. Electroanal. Chem. 199 (1986) 351.
[12] R.R. Adžić, in: J. Lipowski, P.N. Ross (Eds.), Electrocatalysis, Wiley-VCH, NY, 1998, p. 197.
[13] M. Metikoš-Huković, R. Babić, J. Piljac, J. New Mater. Electrochem. Syst. 7 (2004) 179.
[14] S. Hadži-Jordanov, H. Angerstein-Kozlowska, M. Vuković, B.E. Conway, J. Phys. Chem. 81 (1977) 2271.
[15] S. Hadži-Jordanov, H. Angerstein-Kozlowska, M. Vuković, B.E. Conway, J. Electrochem. Soc. 128 (1978) 1471.
[16] V. Birss, R. Myers, H. Angerstein-Kozlowska, B.E. Conway, J. Electrochem. Soc. 131 (1984) 1502.
[17] L.D. Burke, J.K. Mulcahy, J. Electroanal. Chem. 73 (1976) 207.
[18] L.D. Burke, T.O. O′Meara, J. Chem. Soc. Faraday Soc. 68 (1972) 839.
[19] D. Michell, D.A.J. Rand, R. Woods, J. Electroanal. Chem. 89 (1978) 11.
[20] M. Vuković, D. Čukman, J. Electroanal. Chem. 474 (1999) 167.
[21] D. Marijan, D. Čukman, V. Vuković, M. Milun, J. Mater. Sci. 30 (1995) 3047.
[22] M. Vuković, T. Valla, M. Milun, J. Electroanal. Chem. 356 (1993) 81.
[23] J. Rishpon, S. Gottesfeld, J. Electrochem. Soc. 131 (1984) 1960.
[24] V. Horvat-Radošević, K. Kvastek, M. Vuković, D. Čukman, J. Electroanal. Chem. 482 (2000) 188.
[25] L.D. Burke, O.J. Murphy, J. Electroanal. Chem. 96 (1979) 19.
[26] V.S. Bagotzky, A.M. Skundin, E.K. Tuseva, Electrochim. Acta 21 (1976) 29.
[27] R. Kötz, S. Stucki, D. Scherson, D.M. Kolb, J. Electroanal. Chem. 172 (1984) 211.
[28] R.O. Lezina, N.R. de Tacconi, A.J. Arvia, J. Electroanal. Chem. 151 (1983) 193.
[29] M. Pourbaix, Atlas of Electrochemical Equilibria in Aqueous Solutions, Pergamon Press, NY, 1966.
[30] D. Galizzioli, F. Tantardini, S. Trasatti, J. Appl. Electrochem. 4 (1974) 57.
[31] K. Doblhofer, M. Metikoš, Z. Ogumi, H. Gerischer, Ber. Bunsenges. Phys. Chem. 82 (1978) 1046.
[32] J.E. Weston, B.C.H. Steele, J. Appl. Electrochem. 10 (1980) 49.
[33] S. Ardizzone, A. Carugati, G. Lodi, S. Trasatti, J. Electrochem. Soc. 129 (1982) 1689.
[34] G.W. Jang, E.W. Tsai, K. Rajeshwar, J. Electroanal. Chem. 263 (1989) 383.
[35] B. Boukamp, Solid State Ionics 20 (1980) 31.
[36] C. Ho, I.D. Raistrick, R.A. Huggins, J. Electrochem. Soc. 127 (1980) 343.
[37] C.M. Elliot, A.B. Kopelove, W.J. Albery, Z. Chen, J. Phys. Chem. 95 (1991) 1743.
[38] S.H. Glarum, J.H. Marshal, J. Electrochem. Soc. 127 (1980) 1467.
[39] T. Amemiya, K. Hashimoto, A. Fujishima, J. Phys. Chem. 97 (1993) 9736.
[40] G. Inzelt, G. Lang, J. Electroanal. Chem. 378 (1994) 39.
[41] J.R. Macdonald (Ed.), Impedance Spectroscopy, Wiley, NY, 1987.
[42] S. Levine, A.L. Smith, Discuss. Faraday Soc. 52 (1967) 1290.
[43] I.D. Raistrick, R.J. Sherman, Proc. Electrochem. Soc. 142 (1987) 582.
[44] E.W. Tsai, K. Rajeshwar, Electrochim. Acta 36 (1991) 27.
[45] Y.V. Pleskov, V.Y. Filinovskii, The Rotating Disk Electrode, Plenum Press, NY, 1976.
[46] K.-L. Hsueh, E.R. Gonzales, S. Srinivasan, Electrochim. Acta 28 (1983) 691.
[47] K.-L. Hsueh, D.T. Chin, S. Srinivasan, J. Electroanal. Chem. 153 (1983) 79.
[48] A. Damjanovic, M.A. Genshav, J.O′M. Bockris, J. Chem. Phys. 45 (1966) 4057.

Editor's Note

After correcting the proofs and with the corrected paper available on the web, the Authors of this work realized that appropriate reference to two previous papers was missing.

The two papers are:

A V. Horvat-Radošević, K. Kvastek, M. Vuković, D. Čukman, J. Electroanal. Chem. 482 (2000) 188.
B K. Kvastek, V. Horvat-Radošević, J. Electroanal. Chem. 511 (2001) 65.

These two references are to be introduced as follows:

-p. 1 right, line 10 . . ..[4,5,14–25 + A + B]
-p. 2 left, line 6 . . ..[23,24 + A + B]
-p. 4 left, line 14 . . ..a hydrous oxide [19,23]. While. . ..
-p. 4 left, line 21 . . ..impedance analysis [23,24 + A + B]
-p. 4 right, line 9 . . ..in Fig. 3, which was developed for electrodeposition of Ru [24]
-p. 4 right, line 14 . . ..EEC is as follows [24]:

The Authors apologize for the inconvenience.

S. Trasatti
Editor-in-Chief